

Experimental campaign of horizontal cladding wall panels connection in industrial precast reinforced concrete buildings

September 2024

Liana Ostetto, Jorge Fonseca, Romain Sousa, Paulo Fernandes and Hugo Rodrigues.

The first author acknowledged FCT—
Fundação para a Ciência e a Tecnologia—
namely through the PhD grant of the first
author with reference 2020.08152.BD, DOI
10.54499/2020.08152.BD.

Table of Contents

1. Introduction	3
2. Experimental campaign test program.....	6
2.1. Introduction and objectives	6
2.2. Test Setup	6
2.3. Specimens design	8
2.4. Load protocol and instrumentation	11
3. Experimental test results	14
3.1. In-plane tests	14
3.1.1. Force-displacement hysteretic curves	14
3.1.2. Friction	15
3.1.3. Dissipated energy	17
3.1.4. Observed Damages.....	18
3.2. Out-of-plane tests	20
3.2.1. Force-displacement hysteretic curves	20
3.2.2. Dissipated energy	21
3.2.3. Damages.....	22
4. Final Considerations.....	24
Acknowledgements	25
References.....	26

1. Introduction

In recent years, there has been a concern about how to ensure the safety of existing structures during and after natural events (Batalha et al., 2022) being clearly important to know the different types building typologies to understand their behavior under seismic events (Batalha et al., 2019). Industrial precast reinforced concrete (PRC) buildings are a common typology found in European industrial parks (Batalha et al., 2019; Del Monte et al., 2019), most of them using solution of façades with vertical and horizontal precast cladding panels. In the Portuguese industrial park, the most current arrangement of cladding panels observed in PRC buildings is the horizontal one (Babič & Dolšek, 2016; Belleri et al., 2015; Rodrigues et al., 2020), that are also recognized as the most vulnerable (Belleri et al., 2014; Ercolino et al., 2014; Zoubek et al., 2016). The arrangement consists of precast cladding panels usually fixed by four connections of each panel and to the columns (Figure 1 Figure 2). These connections should comply with the specifications of EN 1998 – 1 (Eurocode 8: Design of Structures for Earthquake Resistance. Part 1: General Rules, Seismic Actions and Rules for Buildings, 2004) and EN 1992-1-1 (Eurocode 2 - Design of Concrete Structures. Part 1 - 1: General Rules and Rules for Buildings, 2004).



Figure 1 - Typical Portuguese industrial building with horizontal cladding panels.

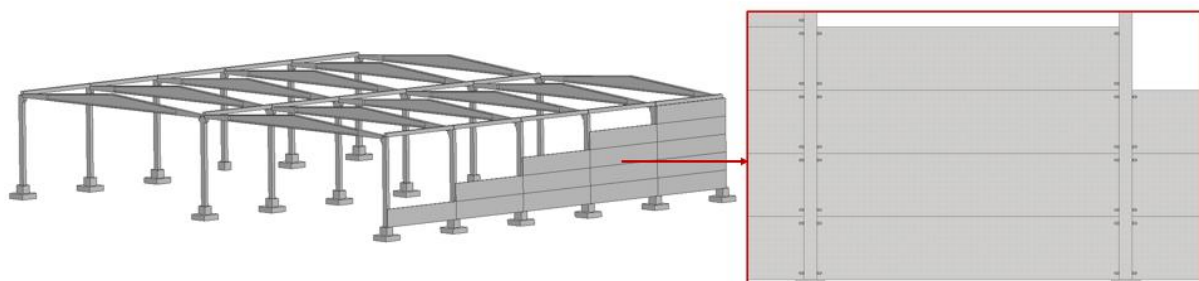


Figure 2 – Three-dimensional overview of an industrial PRC building with façade panels and associated connections.

During recent earthquakes in Italy and Turkey, several precast buildings have exposed their vulnerability, highlighting structural and non-structural damages, most related to deficient transferring of horizontal forces, namely in the connections between elements (Arslan et al., 2024; Batalha et al., 2019; Sagbas et al., 2024). According to Del Monte et al (Del Monte et al., 2019), Italian earthquakes, such as L'Aquila 2009 and Emilia 2012, have emphasized some critical issues in the behavior of cladding-to-structure devices used in the past (Figure 3). The damage observed in these recent earthquakes showed that these elements can have a significant contribution on the structural behavior of the building and should be considered when designing the structure (Arslan et al., 2024; Batalha et al., 2019; Bellotti et al., 2023; Lamperti Tornaghi et al., 2022; Magliulo et al., 2015; Ostetto et al., 2021, 2023). Cladding-to-structure connections play key roles in the safety, performance, and economics of both the cladding system as well as the main structure itself (Del Monte et al., 2019).



Figure 3 – Precast cladding failures.

After the past earthquakes, several significant experimental works have been developed to mitigate the problems of the connections. Relevant studies on the in-plane seismic performance of cladding panels, typically adopted in PRC buildings, were published recently. Belleri et al. (Andrea Belleri et al., 2016) emphasize the seismic performance of horizontal panels with different connections at the top and bottom of the panel, however, Zoubek et al. (Zoubek et al., 2016) and Isakovic et al. (Isakovic et al., 2017) focus on connections used in the vertical or horizontal panels to beams. Many experimental works were developed in the scope of the *Safecladding* project (Colombo et al., 2014; Isaković et al., 2014), especially for new technological solutions (Colombo et al., 2016; Dal Lago et al., 2017a; Dal Lago &

Lamperti Tornaghi, 2018a; Negro & Lamperti Tornaghi, 2017; Scalbi et al., 2018; Toniolo & Lago, 2017). Another assessment of in-use commercial fastenings was carried out by Del Monte et al. (Del Monte et al., 2019), the experimental campaign focused on the Isostatic Sliding-Frame system for both horizontal and vertical panels, with in-plane and out-of-plane load application, in addition to proposing and testing a new connection solution.

After the literature review and considering the specific properties of the industrial building stock (Rodrigues et al., 2020; Sousa et al., 2020), it was noticed that there was a lack of study of the connections commonly used in Portugal. These connections differ from those used in other countries, mainly due to the steel angle plate used without reinforced rib. In addition to the fact that cantilever connections or channels in both the panel and the column are widely used in other places. Another difference identified is the use of different connections at the top and bottom of the panel.

This study focuses is on one of the most typical existing cladding-to-columns standard connections. The objective was to develop an experimental campaign in the laboratory, to investigate the in-plane and out-of-plane performance in connections of horizontal precast reinforced concrete cladding panels in a typical Portuguese PRC industrial building.

2. Experimental campaign test program

2.1. Introduction and objectives

Experimental tests are essential for understanding the behavior of each component, particularly the cladding-to-columns connection. The main objectives of this experimental research are to gain a deeper understanding of the commonly used connections in Portugal and to obtain reliable results.

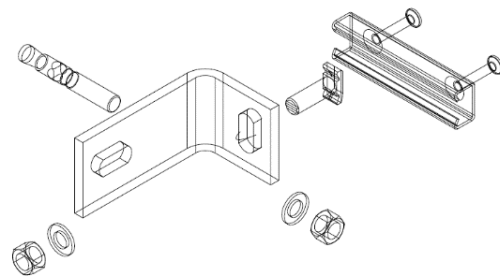
This section describes the experimental campaign conducted. The experimental setups were designed based on recent studies by the authors Del Monte et al. (Del Monte et al., 2019), Belleri et al. (Andrea Belleri et al., 2016), Zoubek et al. (Zoubek et al., 2016) and Isakovic et al. (Isakovic et al., 2017), and in accordance with the recommendations for quasi-static cyclic tests set forth in FEMA 461 (FEMA 461, 2007). The present section describes the experimental programs, namely the test setups, the specimens detailing, the materials adopted, the load control and the instrumentation scheme.

2.2. Test Setup

The experimental campaign is focused on the configuration of Isostatic Sliding-Frame for horizontal panels. This type of non-load-bearing connection is usually composed of anchor channels pre-installed in the panels, steel angle plate fixed with a hammerhead bolt, nuts, washers, and bolts to fix the steel angle plate on the columns. The hammerhead bolts are for anchoring the channels and they are provided with sliding blocks to prevent them from locking, so that they can slide freely inside the channel profile. (Figure 4).



a)



b)

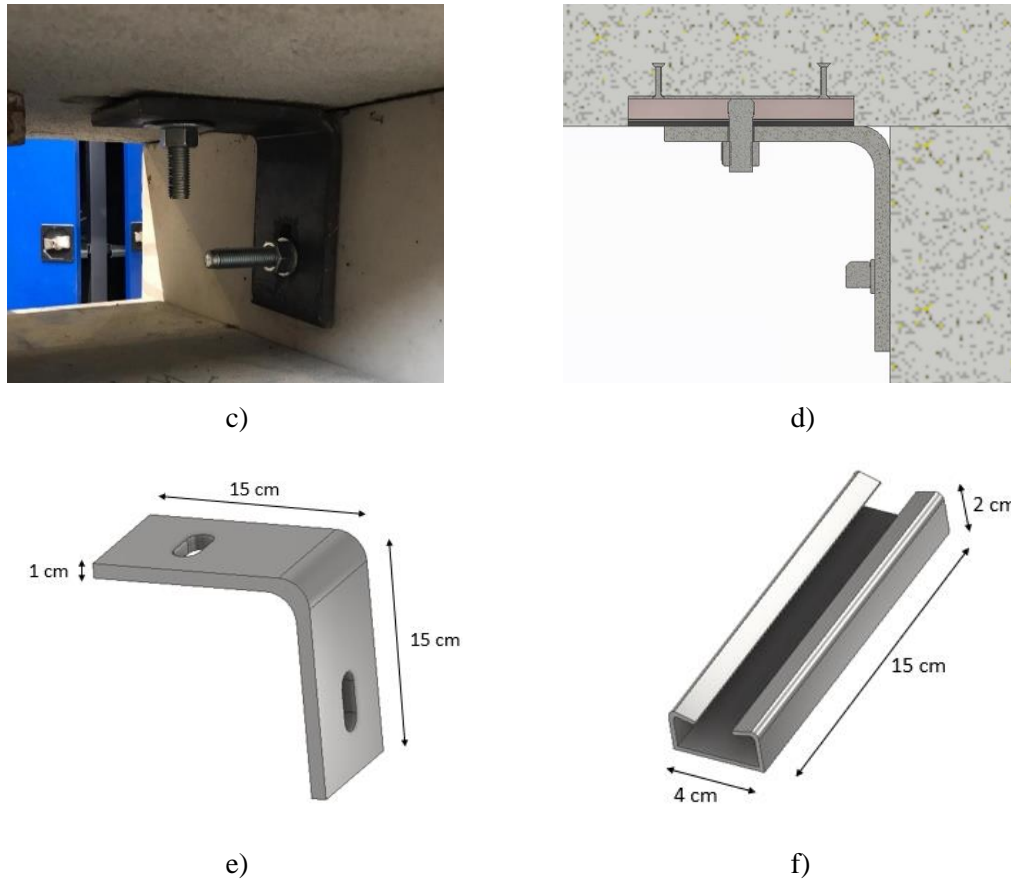


Figure 4 - Details of cladding-to-column connection: a) Commonly used connection; b) Connection accessories; c) Connections used in the tests; d) Front view of the connection; e) Steel angle plate dimensions; f) Channel dimensions.

Two test systems were developed to characterize the in-plane (Figure 5) and out-of-plane (Figure 6) behavior of the cladding-to-column connection. The detail of the specimens was established through the work of the typical properties of Portuguese industrial precast buildings presented by Rodrigues et al. (Rodrigues et al., 2020) to represent a cladding-to-column connection of a typical Portuguese industrial PRC building. The tests are based on quasi-static cyclic tests of the hysteretic type, according to recommendations of FEMA 461 (FEMA 461, 2007). The connection is located at the end of the panel with the column. To ensure the fixation of the column, it was fixed to the reaction slab with a prestressing of 400kN in all the tests.

The in-plane tests (Figure 5) were carried out through a horizontal displacement imposed by a hydraulic actuator with a maximum capacity of 200 kN and ± 400 mm stroke. The actuator was positioned to be centered horizontally with the connection.

The out-of-plane tests (Figure 6) were carried out through a vertical displacement imposed by a hydraulic actuator with a maximum capacity of 200 kN and a stroke of ± 200 mm. The actuator was positioned vertically, to be centered with the connection.

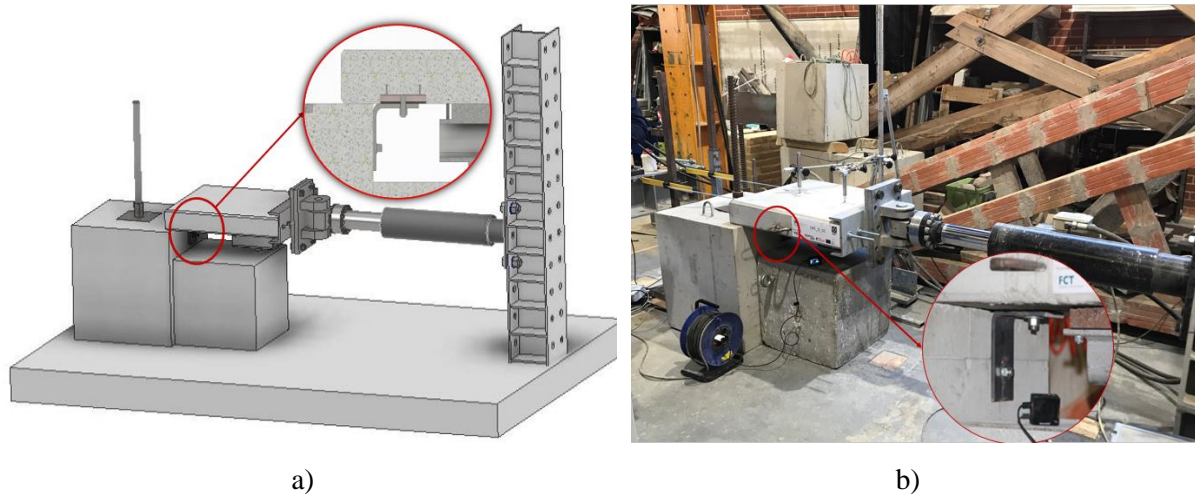


Figure 5 – Schematic testing of the cladding-to-column connection in-plane: a) Test scheme; b) General view.

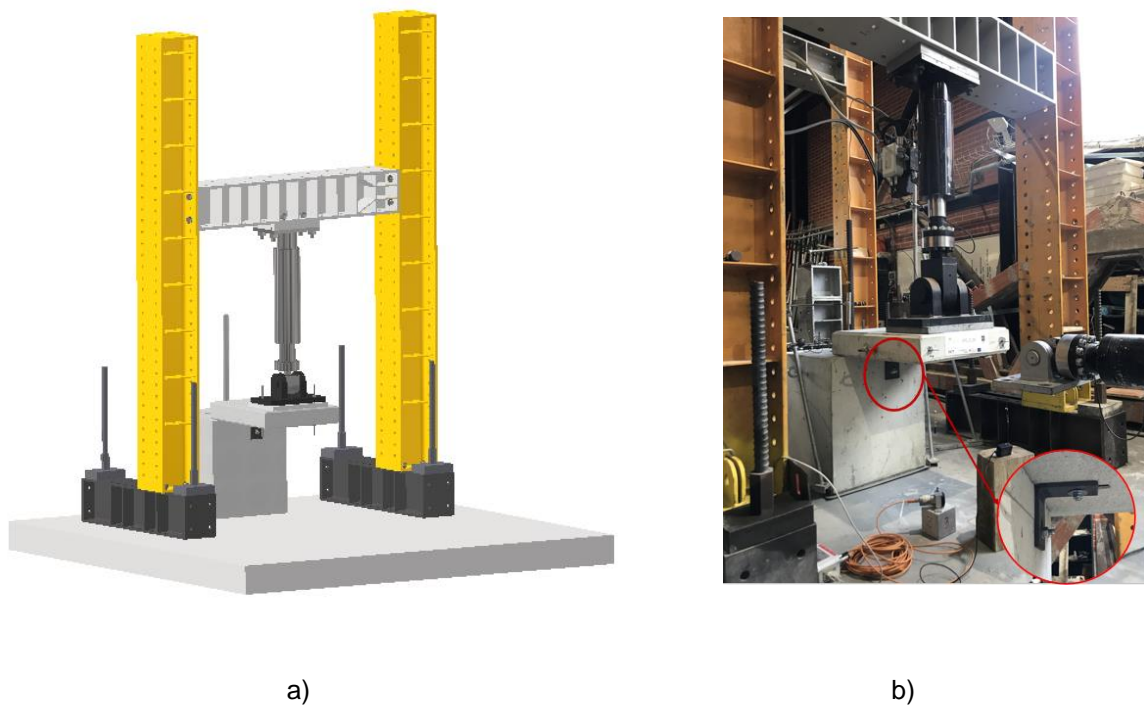


Figure 6 - Schematic testing of the cladding-to-column connection out-of-plane: a) Test scheme; b) General view.

2.3. Specimens design

The experimental specimens, namely the column and panel, were built to full scale and represent the connection region between the panel and the column.

The detailing of the columns is presented below in the Figure 7. The columns have a rectangular cross section of $0.60 \times 0.60 \text{ m}^2$ with 0.68 meters high, the longitudinal reinforcement comprises eight 20 mm diameter bars and, on the transverse reinforcement, of 8 mm diameter stirrups spaced at 0.10 m. All the

specimens have a 25 mm of cover. The columns have been fixed through a 40 mm diameter bar from the specimen's center to the reaction floor.

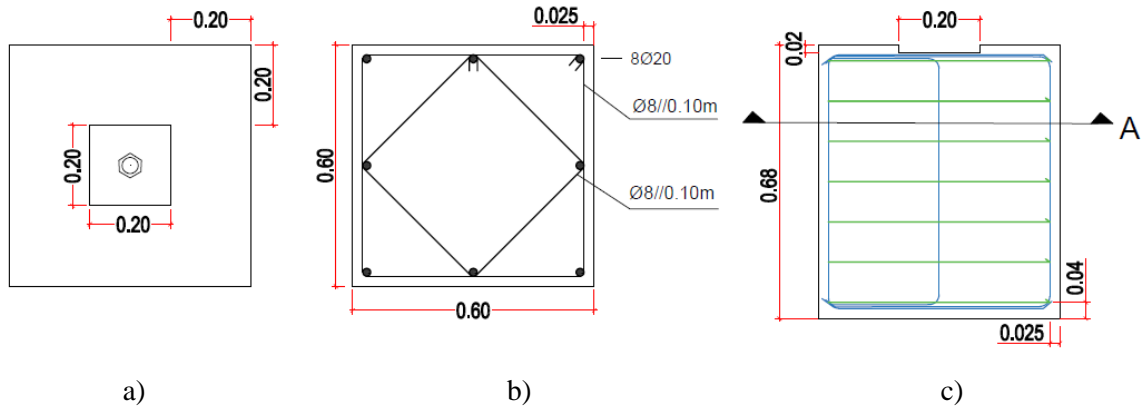


Figure 7 - Columns detailing: a) Top view; b) Section A; c) Front view.

Regarding the panel, a fraction of the facade panel was considered (0.12x0.7x0.6m), corresponding to the model typically adopted for facade panels of 12cm thickness, present in Figure 8.

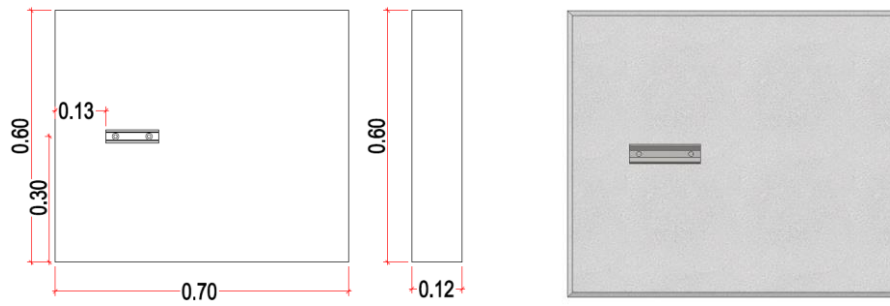


Figure 8 - Panel detailing.

The nomenclature employed for each specimen is “CPC_O_xx,” where 'xx' signifies the test sequence, as various tests were conducted with different bolt tightening levels. A more detailed nomenclature was later adopted: “CP_CTz_L_XXy,” where 'z' indicates the bolt tightening level, 'L' refers to the load protocol type (either 'I' for incremental load or 'S' for sinusoidal load), 'XX' represents the test type (either 'IP' for in-plane tests or 'OOP' for out-of-plane tests), and 'y' denotes the test sequence.

For the in-plane tests, the first scenario aimed to understand the friction between elements with the bolt untightened (CP_CT0_I_IP1). Subsequent tests simulated medium torque tightening of the connection bolts (e.g., CP_CT50_I_IP5). The final scenario simulated ideal conditions with maximum tightening, using the highest torque recommended by the manufacturer (e.g., CP_CT100_I_IP6).

A separate group of tests was conducted to study the out-of-plane behavior of the panels. Two different bolt tightening levels were examined, namely medium torque and maximum torque, in order to connect the panel to the angle plate.

Table 1 provides a summary of the properties associated with each specimen type, specifically the type of test, the specimen name, the connection information and load protocol. The channel location, defined as the longitudinal distance from the end of the panel to the beginning of the channel has a value of 0.13 cm (containing manufacturing variation), as illustrated in Figure 8. The tests always start with the bolt positioned halfway along the channel (Figure 5), with a maximum displacement capacity of 7.5 cm .

Table 1 - Specimens properties

	Specimens Name	Tests Name	Connection		
			Channel bolt tightening (N.m)	Column bolt tightening (N.m)	Load Protocol
In-plane	CPC_O_01	CP_CT0_I_IP1	0	75	Increase
	CPC_O_02	CP_CTM_I_IP2	Medium (no control)	75	Increase
	CPC_O_03	CP_CT100_I_IP3	100	100	Increase
	CPC_O_04	CP_CT50_I_IP4	50	110	Increase
	CPC_O_05	CP_CT50_I_IP5	50	Higher (no control)	Increase
	CPC_O_06	CP_CT100_I_IP6	100	110	Increase
	CPC_O_07	CP_CT100_S_IP7	100	100	Sinusoidal
	CPC_O_08	CP_CT50_S_IP8	50	100	Sinusoidal
	CPC_O_14	CP_CT100_I_IP14	100	100	Increase
	CPC_O_15	CP_CT50_I_IP15	50	100	Increase
	CPC_O_16	CP_CT50_I_IP16	50	100	Increase
	CPC_O_17	CP_CT100_I_IP17	100	100	Increase
Out-of-plane	CPC_O_09	CP_CT100_I_OOP9	100	100	Increase
	CPC_O_10	CP_CT50_I_OOP10	50	100	Increase
	CPC_O_11	CP_CT100_S_OOP11	100	100	Sinusoidal
	CPC_O_12	CP_CT100_I_OOP12	100	100	Increase
	CPC_O_13	CP_CT50_I_OOP13	50	100	Increase

The materials considered in the specimens were based on the concrete and reinforcement of the existing PRC Portuguese industrial building (Rodrigues et al., 2020). The concrete used in the column and facade panel was of strength class C40/50 and C30/37 respectively, while the reinforcing steel was of strength class S500 for both elements.

The connection comprises an M16 bolt for securing the steel angle to the column and an M16 T8.8 hammerhead bolt for anchoring the channels. To obtain precise data on the properties of the steel angle (Figure 4e) used, tensile tests were conducted on two specimens cut from the steel angle. The specimens measured 10.08 mm in width and 0.3 mm in thickness. The test results were employed to generate simplified material models of stress (σ) versus strain (ϵ) curves. The tests validated that the material

corresponded to the S275 steel class. The stress-strain diagram of the steel specimens is presented in Figure 9.

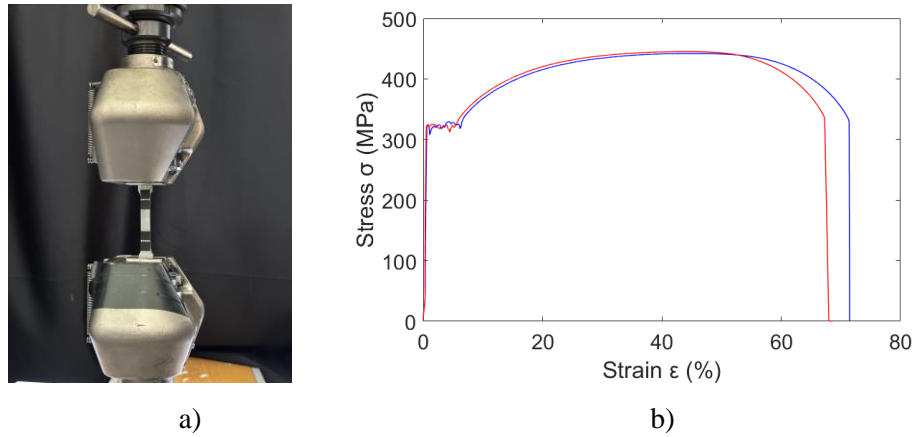


Figure 9 - Material property diagram of steel angle: a) Tensile Test; b) Stress(σ)-Strain (ϵ) curves.

2.4. Load protocol and instrumentation

The specimens were tested under imposed displacements in two directions: horizontal (parallel to the panel channel) for in-plane tests and vertical (perpendicular to the panel channel) for out-of-plane tests. Two types of displacement histories were applied to the panels: one with an increasing amplitude and another with a sinusoidal displacement path.

For the cyclic loading protocol applied with a sinusoidal cyclic displacement increasing amplitude, displacements history at frequency of 0.01 Hz. This displacement history was designed to capture stiffness and strength degradation through cycle repetition. Each displacement level was repeated three times, with increments from 0 to 5 mm in 1 mm steps, from 5 to 20 mm in 5 mm steps, and from 20 to 100 mm in 10 mm steps (see Figure 10a). The test protocol and velocities are similar to the tests performed on friction connections used by different authors (Dal Lago et al., 2017b; Dal Lago & Lamperti Tornaghi, 2018), where was also verified that cyclic tests performed with a reduced speed reach very similar results with respect to those performed at full speed.

For the sinusoidal cyclic loading, displacements were applied at a frequency of 0.025 Hz with a displacement of 50 mm. The objective of this test was to capture stiffness and strength degradation through continuous repetition without contact with the concrete (see Figure 10b).

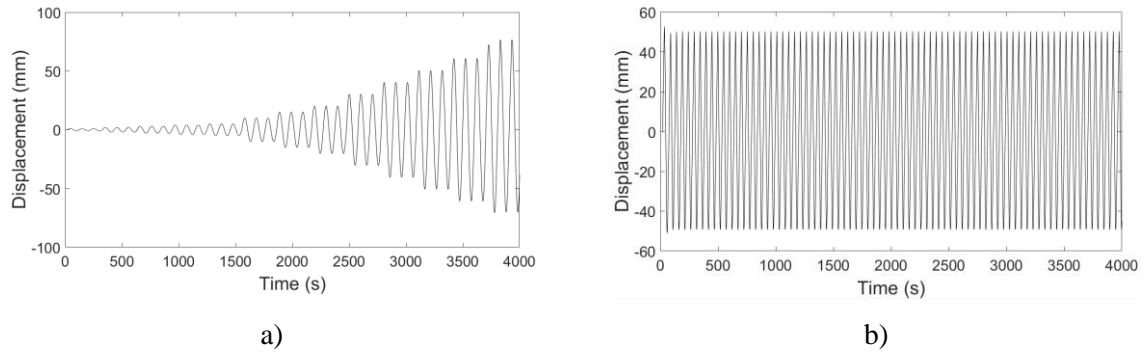


Figure 10 - Imposed displacement-time histories: a) Increase in amplitude; b) Sinusoidal.

The imposed load was monitored through a load cell, and the applied displacement was measured using external displacement transducers. The instrumentation scheme adopted for in-plane tests is presented in Figure 11. Two displacement transducers (LVDT) were positioned at the top of the panel to control the rotation (Figure 11b), and another two on the side of the panel to control the displacement (Figure 11a). An extra LVDT was positioned at column level to control possible elevation/rotation of the column lateral.

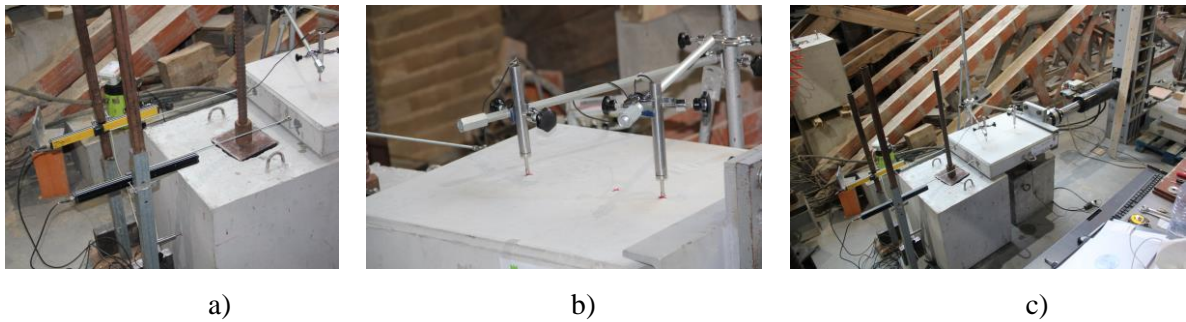


Figure 11 - Displacement instrumentation scheme adopted in the in-plane test a) Transducers on the side of the panel; b) Transducers at the top of the panel; c) General view.

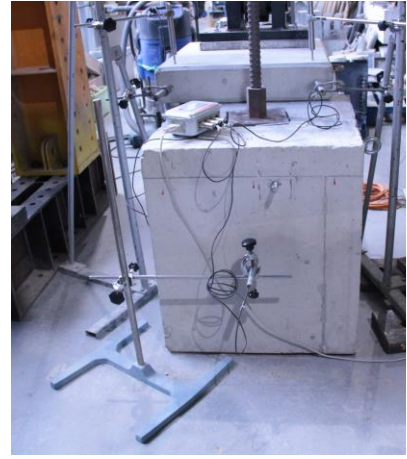
For the out-of-plane tests, two LVDTs were used on the front side of the panel to control the displacement (Figure 12a), a further two on the top of the panel and two on the side of the panel to control the rotation (Figure 12b). An additional LVDT was positioned at the column level to check any column lift/rotation (Figure 12c).



a)



b)



c)

Figure 12 - Displacement instrumentation scheme adopted in the out-of-plane test: a) Transducers on the front side of the panel; b) Transducers on the top and side of the panel; c) Transducer at the column.

3. Experimental test results

This section presents the results of the experimental campaign, starting with a discussion of the force-displacement hysteretic curves, followed by the friction coefficients for each tightening level, and the energy dissipated in each test. In addition, the most representative damage observed in each test specimen is presented and compared between the different tests.

3.1. In-plane tests

3.1.1. Force-displacement hysteretic curves

The force-displacement hysteretic curves obtained from the in-plane experimental tests are shown in Figure 13. The curves have been grouped according to the displacement imposed and the level of tightening .

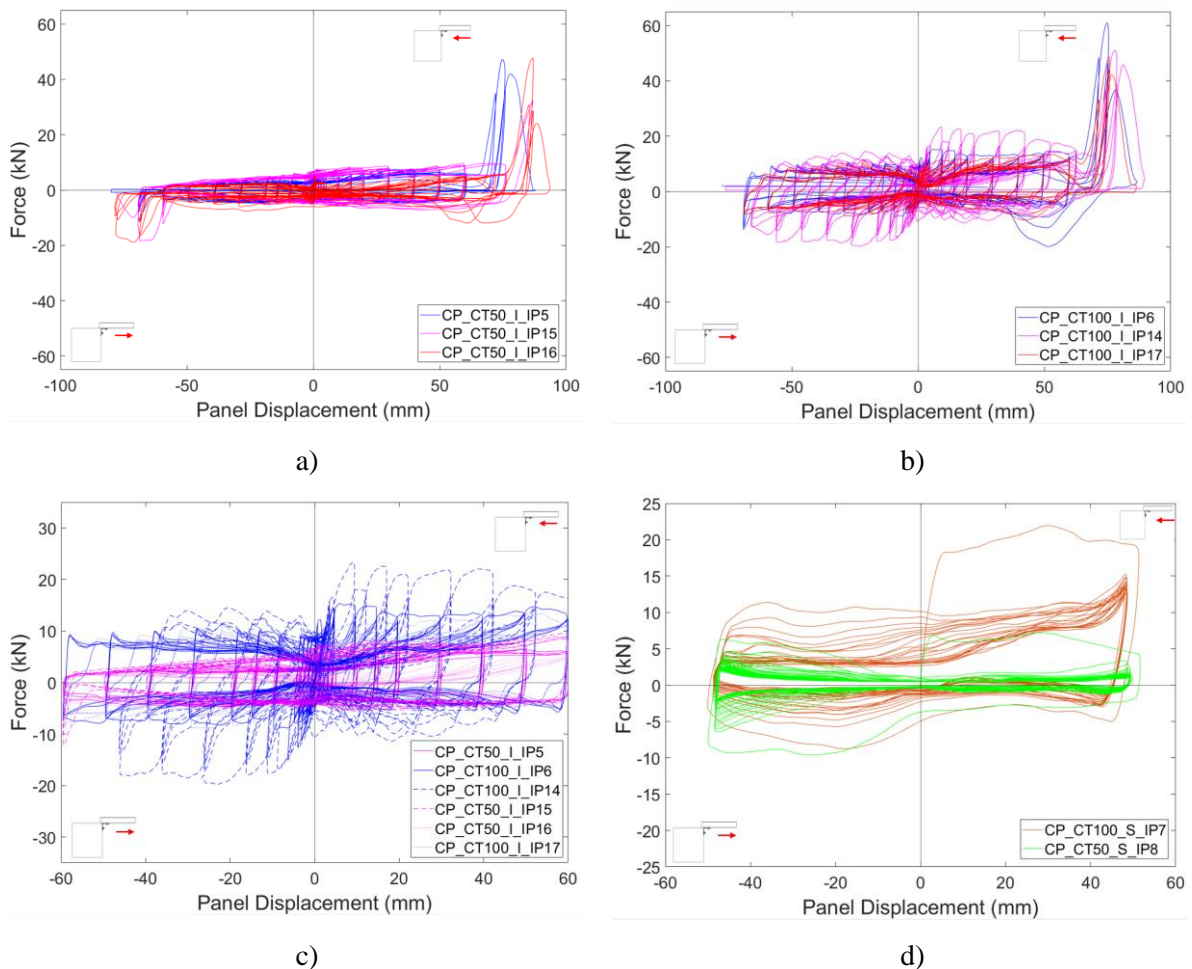


Figure 13 - Force-displacement curves from in-plane tests: a) 50 N.m tightness; b) 100 N.m tightness; c) Increased displacement amplitude; d) Sinusoidal displacement.

The tests CP_CT0_I_IP1, CP_CTM_I_IP2, and CP_CT100_I_IP3 were carried out sequentially on the same specimens. The purpose of the CP_CT0_I_IP1 test was to demonstrate that there was no significant

friction between the elements and to observe how sliding occurs in the channel without tightening the hammerhead bolt.

The first characteristic of the curves shown is their asymmetric shape. This asymmetry arises because the connection behaves differently depending on the direction of the applied displacement. This effect is mainly due to the fact that besides the angle is in contact and tightened against the column from the beginning; due to the cyclic load, when the angle is pulled in the opposite direction of the column, there is a bending of the angle, which does not occur in the opposite direction, when the angle is pushed against the column. This phenomenon becomes more significant as the cyclic action progresses and as the bolt connecting the angle to the column loosens.

During the tests, the sliding of the hammerhead bolt inside the channel was visible, as shown by the hysteretic curves. In the 50 N.m, torque tests, the angle plate is less stressed due to lower tightness, allowing the bolt to slide more easily in the channel. As the hammerhead bolt is tightened more, the force required increases, but the maximum strength of the connection does not change significantly. Failure of the connection occurs only when the full displacement range is exceeded. The hysteretic curves (Figure 13c) show that depending on the bolt tightening, the applied force can increase more than threefold for certain displacements. In sinusoidal load tests (Figure 13d), the maximum displacement achieved was 50 mm, without any failure of the connection being observed.

Figure 13a and Figure 13b highlight that, despite identical test conditions for the three tests with the similar torque level, the force-displacement curves are similar but not identical. This variation can be attributed to several factors such as manufacturing issues in the channel, but the main reason should be linked with the in real torque value applied, which was applied to the bolt, tightening the angle to the channel in the cladding pane that was introduced with a common torque wrench. This manual application clearly induced different levels of torque, that induces a high variability of the results. No connection failure was observed in the CP_CT100_S_IP7 and CP_CT50_S_IP8 tests.

3.1.2. Friction

This subsection presents and discusses the friction observed in in-plane tests. During the test, it was observed that the force transmitted by the connection is mainly due to the friction that arises, during sliding, between the steel angle plate and the washer of the hammerhead bolt. Therefore, the friction force can be represented by its coefficient μ , calculated by dividing the in-plane force acting on the panel F_P (Figure 13) by the out-of-plane force imposed by the connection F_C , as determined by the following expressions:

$$\mu = \frac{F_P}{F_C} \quad (1)$$

$$F_C = \frac{T}{K \times d} \quad (2)$$

where, T is the hammerhead bolt tightness, K is a constant that depends on the bolt material and size, assumed to be 0.2, and d is the bolt diameter. Figure 14 shows the friction of in-plane tests, differentiated by bolt tightness. It should be mentioned that after 60/70 mm, the hammerhead bolt reached the end of the channel and, for this reason, the force observed was no longer correlated to the friction.

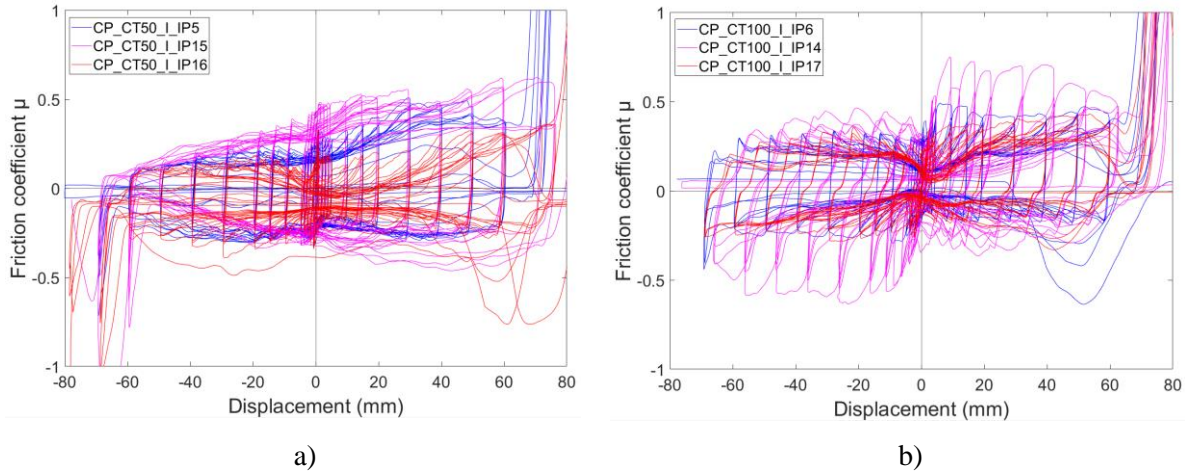
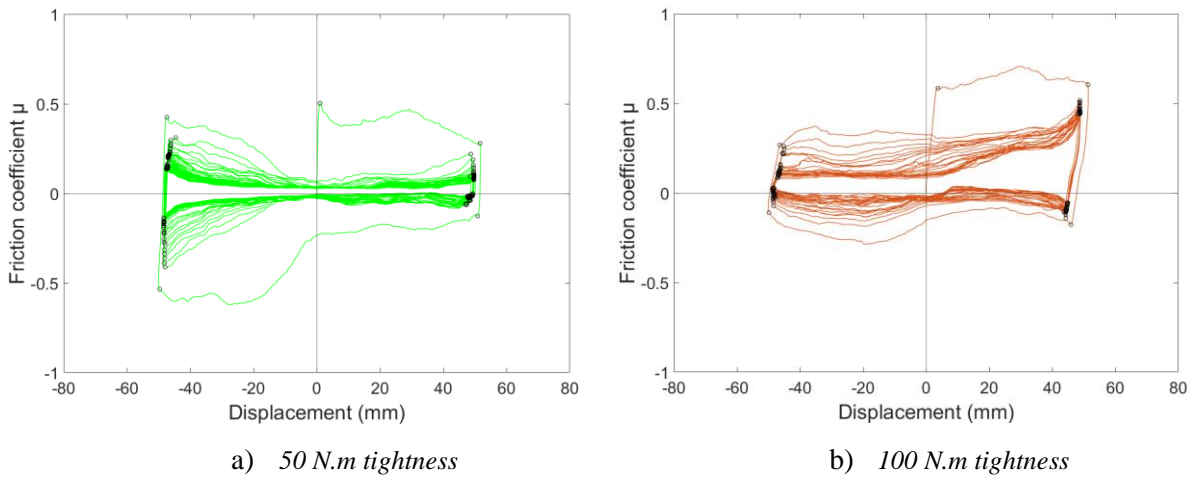


Figure 14 - Friction-displacement curves from in-plane tests: a) 50 N.m tightness; b) 100 N.m tightness.

The friction static μ_s and dynamic μ_D coefficients were evaluated from the friction-displacement curves with sinusoidal imposed displacement. The static coefficient is calculated at the points where the absolute value of the force is maximum, while the dynamic coefficient is calculated at the points where the displacement is zero, as shown in Figure 15. The dynamic coefficient is represented in the figure by positive and negative averages. Figure 15c and 15d show the friction versus time curves for both tests. The red dashed line highlights the trend of the mean μ values, and the black dashed line highlights the trend of the maximum μ values.



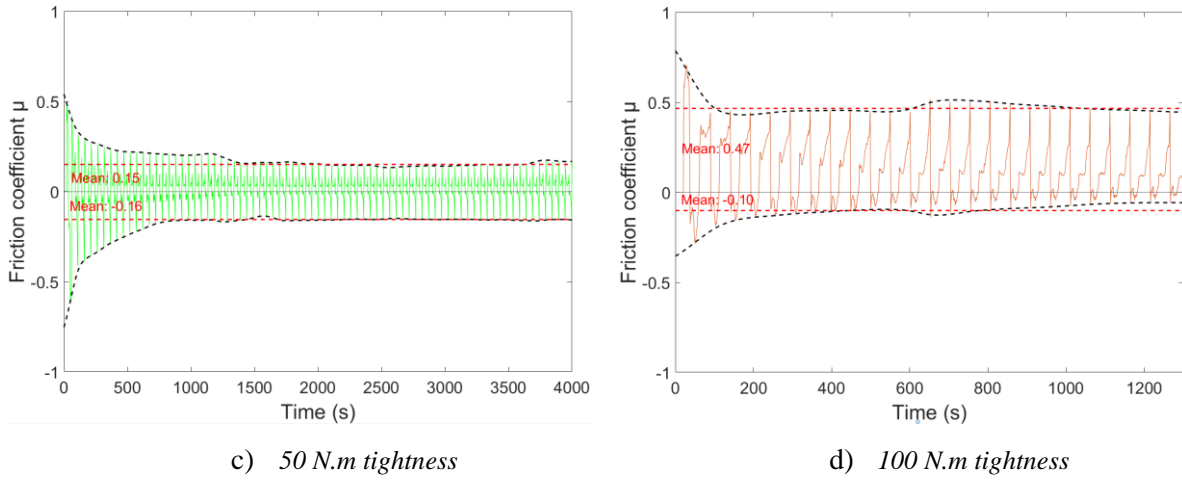


Figure 15 – Friction-displacement and friction-time curves from in-plane tests, of sinusoidal loads with static and dynamic coefficients of friction:

The average static coefficient for the test with 50 N.m tightness in the hammerhead bolt was 0.13, while the average dynamic coefficient was 0.02. For the test with 100 N.m tightness in the hammerhead bolt, the average static and dynamic coefficients were 0.19 and 0.1, respectively.

Both the static and dynamic friction coefficients demonstrated a reduction over time, which can be attributed to the wear of the contact surfaces between the channel, steel angle plate and hammerhead bolt.

With regard to the friction-time curves, the difference between bolt tightness, both in terms of overall shape and values, is confirmed here. During the test with higher tightness, the friction coefficient declines rapidly from approximately 0.78 to 0.43 and stabilizes as shown in Figure 15d. Conversely, in the case of the test with medium tightness, the friction coefficient decreases gradually and reached a stable value of approximately 0.15 after 1400 seconds (Figure 15c).

In conclusion, the experimental results obtained show a correlation between the static and dynamic friction coefficients and the tightening of the hammerhead bolt, with an increase in both as a function of bolt tightness.

3.1.3. Dissipated energy

This subsection presents and discusses the dissipated energy observed in in-plane tests. Figure 16 illustrates the curves corresponding to all tests with increased displacement amplitude, showcasing the accumulated dissipated energy throughout the tests. The dissipated energy was calculated by summing the interior area of the force-displacement cycles.

These findings show that the energy dissipation capacity increases with higher bolt tightening. On average, there is a 25% increase in accumulated dissipated energy at the beginning of the test and a 40% increase by the end of the test with increased bolt tightening.

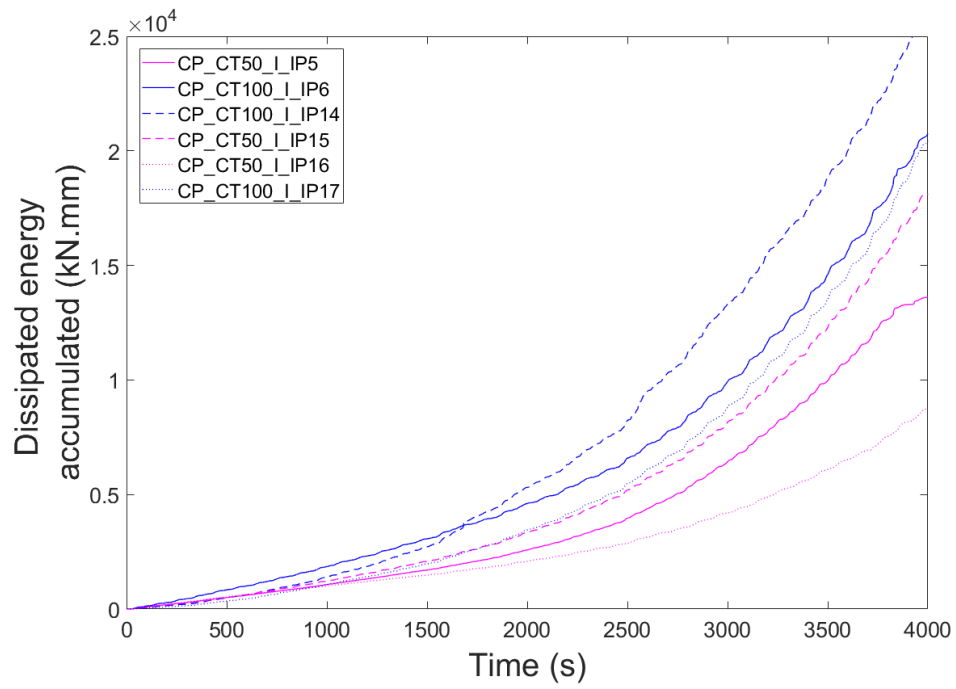


Figure 16 - Dissipated energy in-plane tests.

3.1.4. Observed Damages

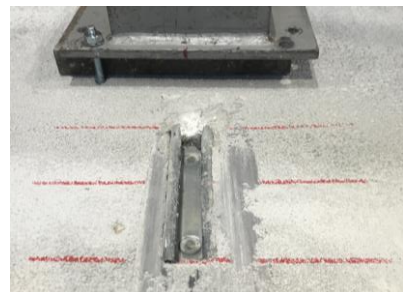
The most representative damages observed in each specimen from in-plane tests are presented in Figure 17, in the respective order of the tests.



a)



b)



c)



d)



e)



f)



Figure 17 - Damages in the specimens from in-plane tests: a) Deformation of the angle plate CP_CT50_I_IP5; b) Failure of the channel CP_CT50_I_IP5; c) Panel after failure CP_CT50_I_IP5; d) Collapse of the anchor channel CP_CT100_I_IP6; e) Failure of the channel CP_CT100_I_IP6; f) Panel after failure CP_CT100_I_IP6; g) Channel deformation, no failure CP_CT100_S_IP7; h) Channel deformation CP_CT100_S_IP7; i) Angle plate not damaged CP_CT100_S_IP7; j) Failure of the channel CP_CT100_I_IP14; k) Collapse of the anchor channel CP_CT100_I_IP14; l) Panel after failure CP_CT100_I_IP14; m) Failure of the channel CP_CT50_I_IP16; n) Failure of the channel CP_CT50_I_IP16; o) Collapse of the anchor channel CP_CT50_I_IP16.

The in-plane tests were carried out until the hammerhead bolt was expelled in the end of the canal. With increased displacements, plastic deformations were observed in the channel pre-installed in the panel, particularly when the bolt slides through the entire channel and came into contact with the concrete. Additionally, deformations in the steel angle plate were observed at larger displacements when the panel is pushed, resulting in contact between the hammerhead bolt and the concrete and subsequent lifting of

the panel (see Figure 17a). It can be seen that failure of the pre-installed channel in the panel is the cause of the connection failure, as illustrated in Figure 17b, 17e, 17f, 17j and 17n, leading to the hammerhead bolt being pulled out of the channel (see Figure 17d, 17k and 17o). Overall, based on the observed damages, the tested connection demonstrates good in-plane behavior for both high and medium tightening levels. In the sinusoidal tests, no failures were observed in the connections, only some deformations in the channel, as shown in Figure 17g, 17h and 17i.

In summary, the tested connection does not exhibit poor in-plane behavior for either high or medium tightening. Damages only occur when the maximum displacement of the channel is reached.

3.2. Out-of-plane tests

3.2.1. Force-displacement hysteretic curves

The force-displacement hysteretic curves obtained in the out-of-plane tests are shown in Figure 18. The curves are grouped according to the imposed displacement with different tightening levels. These tests were conducted to characterize the out-of-plane behavior of the connection. The displacement in these tests was applied up to the maximum allowed by the actuator, which was approximately 60 mm. The curves were also evaluated in terms of moment and rotation, based on the distance between the connection and the location where the actuator force is applied (0.425m), and the angle of rotation of the panel.

The first notable characteristic of the curves is their asymmetric shape, which is due to the lifting movement of the panel. This movement requires greater force for displacement in one direction compared to the opposite direction. During the tests, the hammerhead bolt slipped inside the channel, particularly in the test with a tightening of 50 N.m (Figure 18a). In this test, the rotations of the panel were more pronounced, accompanied by deformations of the angle plate and displacement of one of the LVDTs (CP_CT50_I_OOP10). Nevertheless, the connection remained intact and did not exhibit any significant deterioration throughout the course of the tests.

At the end of the tests, it was observed that both the column bolt and the hammerhead bolt had lost their initial tightening tension. In the test with sinusoidal displacement (Figure 18d), the moment at which the hammerhead bolt slides in the channel is clearly evident, with a constant force indicated by variations in the force-displacement curve.

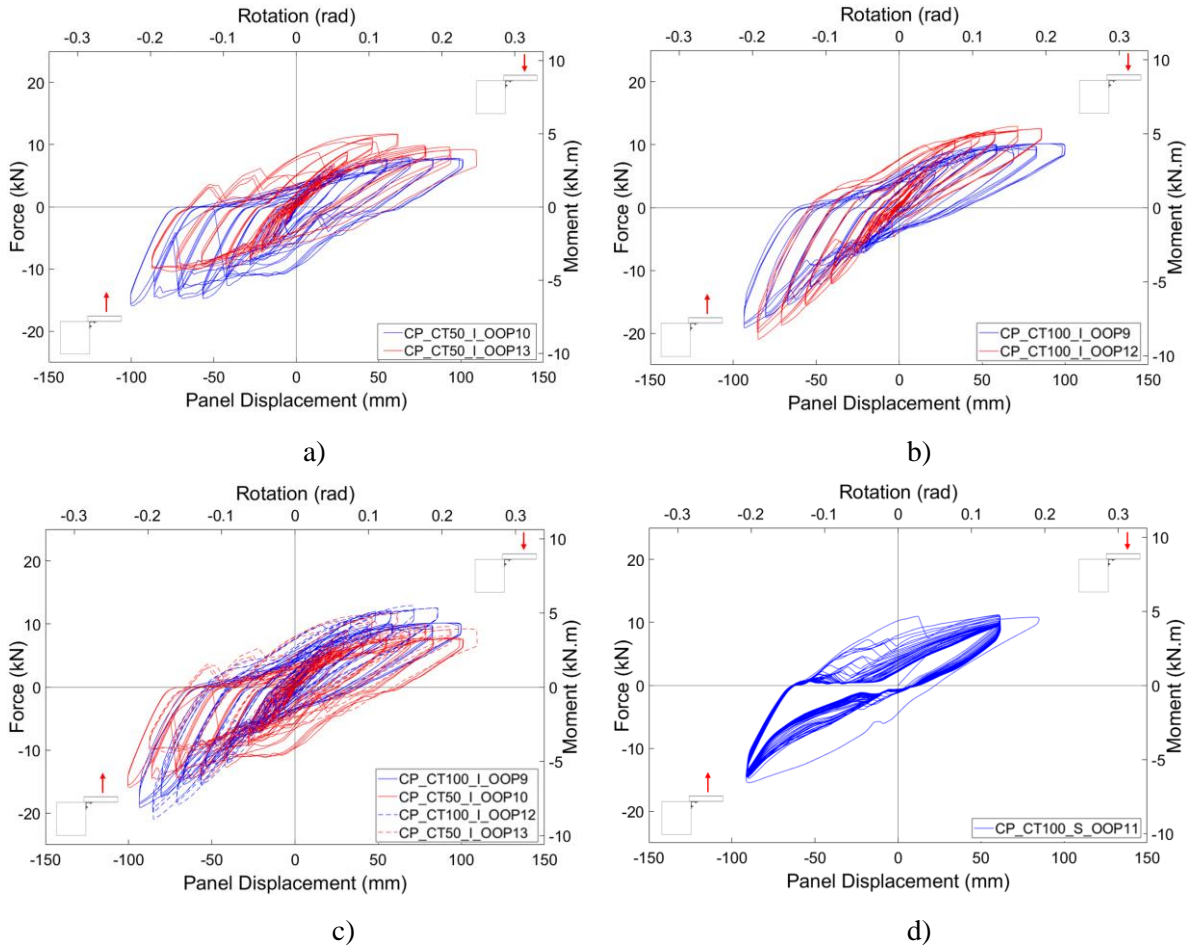


Figure 18 - Force-displacement curves from out-of-plane tests: a) 50 N.m tightness; b) 100 N.m tightness; c) Increased displacement amplitude; d) Sinusoidal displacement.

3.2.2. Dissipated energy

The energy dissipated in the out-of-plane experimental tests is presented and discussed in this subsection. Figure 19 presents the curves corresponding to all tests with increased displacement amplitude, and represents the dissipated energy accumulated throughout the test.

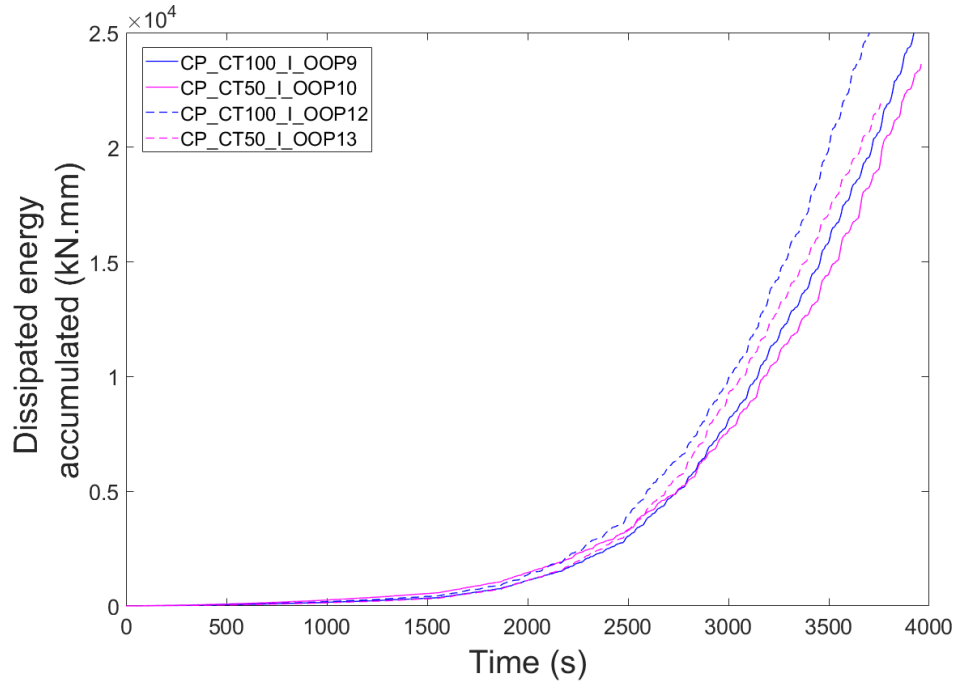


Figure 19 - Dissipated energy from out-of-plane tests

According to the results obtained, the out-of-plane tests also present an increase in the energy dissipation capacity with the increase in bolt tightness. However, the accumulated dissipated energy levels are more similar to those observed in the in-plane tests.

3.2.3. Damages

The most representative damages observed in each specimen are presented in Figure 20, in the order of the tests. In the out-of-plane tests, displacements reached up to 60 mm, which was the maximum allowed by the actuator due to its inclination and force capacity. No failures were observed in the connections during these tests, though some deformations were noted in the pre-installed channel in the panel and the angle plate, as shown in Figure 20. By the end of the tests, it was observed that the hammerhead bolt had lost its tightening tension.

Overall, the tested connection demonstrated good out-of-plane behavior for both high and medium tightening levels.

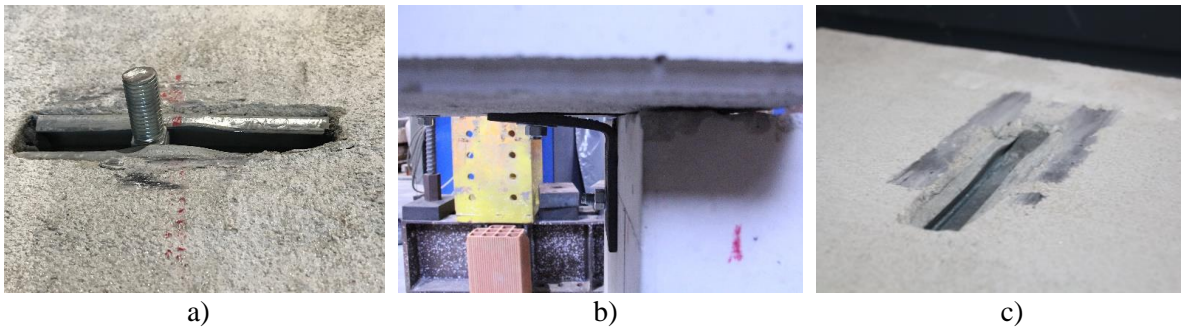


Figure 20 - Damages in the specimens from out-of-plane tests: a) Channel deformation, no failure CP_CT100_S_OOP9; b) Deformation of the angle plate CP_CT50_S_OOP10; c) Channel deformation, no failure CP_CT100_S_OOP11.

4. Final Considerations

The test campaign aimed to study the most common cladding-to-column connection typology in the Portuguese industrial park, specifically in precast industrial structures. This study allowed for an assessment of the connection's behavior under different tightening levels and provided insights into the damage observed in real seismic events in the past.

In the in-plane tests, it was observed that there was no significant friction between the elements when the hammerhead bolt was not tightened in the first test. However, when the subsequent tests were conducted with different levels of tightening, it became evident that the critical importance of tightening the hammerhead bolt inside the channel could not be overstated. The slippage of the hammerhead bolt inside the channel was clearly visible. However, at larger displacements, deformations of the steel angle plate and connection failure were observed. These failures were attributed to plastic deformations of the channel, which occurred when the displacement reached its limit. This resulted in the bolt contacting the concrete and being pulled out of the channel, leading to a collapse of the connection. The hysteretic curves indicated that with high tightness, the applied force could increase up to three times for certain displacements.

Regarding the out-of-plane tests, the connection exhibited satisfactory behavior, with the hammerhead bolt sliding along the entire channel and causing minimal damage, without any connection failures. By the end of the tests, it was observed that the bolts, both on the column and in the channel, had lost their tightening tension.

The experimental results demonstrated a direct correlation between the tightening of the hammerhead bolt and the friction coefficient, as well as the energy dissipated by the connection. While the torque of the hammerhead bolt doubled, the coefficients of friction tripled. Regarding energy dissipation, for the same increase in torque, on average, there was a 25% increase in accumulated dissipated energy at the beginning of the test and a 40% increase by the end of the test. Over time, friction coefficients decreased due to wear on the contact surfaces.

This experimental investigation provided a better understanding of the behavior of this cladding-to-column connection commonly used in Portugal. The findings offer valuable indications on its seismic performance and key parameters for calibrating numerical models. The study concluded that the proper tightening of bolts is of significant importance in maintaining the structural integrity of cladding-to-column connections during seismic events. Furthermore, other issues such as the displacement capacity of the connections should also be taken into account during the design/assessment process.

Acknowledgements

This work was supported by the Foundation for Science and Technology (FCT)-Aveiro Research Centre for Risks and Sustainability in Construction (RISCO), Universidade de Aveiro, Portugal [FCT/UIDB/ECI/04450/2020]. The first author acknowledged FCT—Fundação para a Ciência e a Tecnologia—namely through the PhD grant of the first author with reference 2020.08152.BD, DOI 10.54499/2020.08152.BD.

References

- Arslan, M. H., Dere, Y., Ecemiş, A. S., Doğan, G., Öztürk, M., & Korkmaz, S. Z. (2024). Code-based damage assessment of existing precast industrial buildings following the February 6th, 2023 Kahramanmaraş earthquakes (Pazarcık Mw 7.7 and Elbistan Mw7.6). *Journal of Building Engineering*, 86(February), 108811. <https://doi.org/10.1016/j.jobbe.2024.108811>
- Babič, A., & Dolšek, M. (2016). Seismic fragility functions of industrial precast building classes. *Engineering Structures*, 118, 357–370. <https://doi.org/10.1016/j.engstruct.2016.03.069>
- Batalha, N., Rodrigues, H., & Varum, H. (2019). Seismic performance of RC precast industrial buildings—learning with the past earthquakes. *Innovative Infrastructure Solutions*, 4(1), 1–13. <https://doi.org/10.1007/s41062-018-0191-y>
- Batalha, N., Rodrigues, H., Varum, H., & Arêde, A. (2022). Cyclic behaviour of precast beam-to-column connections with low seismic detailing. *Earthquake Engng Struct Dyn*, January, 1–19. <https://doi.org/10.1002/eqe.3606>
- Belleri, A., Brunesi, E., Nascimbene, R., Pagani, M., & Riva, P. (2014). Seismic performance of precast industrial facilities following major earthquakes in the Italian territory. *Journal of Performance of Constructed Facilities*, 29(5), 1–10. [https://doi.org/10.1061/\(ASCE\)CF.1943-5509.0000617](https://doi.org/10.1061/(ASCE)CF.1943-5509.0000617)
- Belleri, A., Torquati, M., Marini, A., & Riva, P. (2016). Horizontal cladding panels: in-plane seismic performance in precast concrete buildings. *Bulletin of Earthquake Engineering*, 14(4), 1103–1129. <https://doi.org/10.1007/s10518-015-9861-8>
- Belleri, A., Torquati, M., Riva, P., & Nascimbene, R. (2015). Vulnerability assessment and retrofit solutions of precast industrial structures. *Earthquake and Structures*, 8(3), 801–820. <https://doi.org/10.12989/eas.2015.8.3.801>
- Bellotti, D., Cavalieri, F., & Nascimbene, R. (2023). Influence of Closure External Panels Modelling on the Seismic Response of Non-Residential Precast Buildings. *Journal of Earthquake Engineering*, 00(00), 1–17. <https://doi.org/10.1080/13632469.2023.2197517>
- Colombo, A., Lamperti, M., Negro, P., & Toniolo, G. (2016). *Design guidelines for wall panel connections*. <https://doi.org/10.2788/546845>
- Colombo, A., Negro, P., & Toniolo, G. (2014). The influence of claddings on the seismic response of precast structures: the safecladding project. *Proceedings of 2nd ECEES*, 1–12.
- Dal Lago, B., Biondini, F., & Toniolo, G. (2017a). Experimental Investigation on Steel W-Shaped Folded Plate Dissipative Connectors for Horizontal Precast Concrete Cladding Panels. *Journal of Earthquake Engineering*, 22(5), 778–800. <https://doi.org/10.1080/13632469.2016.1264333>
- Dal Lago, B., Biondini, F., & Toniolo, G. (2017b). Friction-based dissipative devices for precast concrete panels. *Engineering Structures*, 147, 356–371. <https://doi.org/10.1016/j.engstruct.2017.05.050>
- Dal Lago, B., & Lamperti Tornaghi, M. (2018). Sliding channel cladding connections for precast structures subjected to earthquake action. *Bulletin of Earthquake Engineering*, 16(11), 5621–5646. <https://doi.org/10.1007/S10518-018-0410-0>
- Del Monte, E., Falsini, C., Boschi, S., Menichini, G., & Orlando, M. (2019). An innovative cladding panel connection for RC precast buildings. *Bulletin of Earthquake Engineering*, 17(2), 845–865. <https://doi.org/10.1007/s10518-018-0470-1>
- Ercolino, M., Magliulo, G., Coppola, O., & Manfredi, G. (2014). Code formula for the fundamental period of RC precast buildings. *Second European Conference on Earthquake Engineering and Seismology*, 1–10.
- Eurocode 2 - Design of Concrete Structures. Part 1 - 1: General Rules and Rules for Buildings, EN 1992-1-1:2004 Comité Européen de Normalisation 259 (2004).
- Eurocode 8: Design of Structures for Earthquake Resistance. Part 1: General Rules, Seismic Actions and Rules for Buildings, EN 1998-1:2004 Comité Européen de Normalisation (2004).
- FEMA 461. (2007). *Interim Testing Protocols for Determining the Seismic Performance Characteristics of Structure and Nonstructural Components* (Issue June).

- Isakovic, T., Zoubek, B., & Fischinger, M. (2017). Design Procedures for Typical Cladding Panel Connections in Rc Precast Buildings. *16th World Conference on Earthquake Engineering*, 12.
- Isaković, T., Zoubek, B., Lopatič, J., & Fischinger, M. (2014). Experimental Research of Typical Cladding Panel Connections in Industrial Buildings. *Second European Conference on Earthquake Engineering and Seismology*, 1–10.
- Lamperti Tornaghi, M., Scalbi, A., & Negro, P. (2022). Precast RC buildings: What is wrong with horizontal cladding panels? *Engineering Structures*, 266, 114456. <https://doi.org/10.1016/J.ENGSTRUCT.2022.114456>
- Magliulo, G., Ercolino, M., & Manfredi, G. (2015). Influence of cladding panels on the first period of one-story precast buildings. *Bulletin of Earthquake Engineering*, 13(5), 1531–1555. <https://doi.org/10.1007/s10518-014-9657-2>
- Negro, P., & Lamperti Tornaghi, M. (2017). Seismic response of precast structures with vertical cladding panels: The SAFECLADDING experimental campaign. *Engineering Structures*, 132, 205–228. <https://doi.org/10.1016/j.engstruct.2016.11.020>
- Ostetto, L., Sousa, R., Fernandes, P., & Rodrigues, H. (2023). Influence and effectiveness of horizontal diaphragms and cladding wall panels on the seismic behaviour of precast RC industrial buildings. *Engineering Structures*, 285, 116046. <https://doi.org/10.1016/J.ENGSTRUCT.2023.116046>
- Ostetto, L., Sousa, R., Rodrigues, H., & Fernandes, P. (2021). Assessment of the Seismic Behavior of a Precast Reinforced Concrete Industrial Building with the Presence of Horizontal Cladding Panels. *Buildings*, 11(9), 400. <https://doi.org/10.3390/BUILDINGS11090400>
- Rodrigues, H., Sousa, R., Vitorino, H., Batalha, N., Varum, H., & Fernandes, P. (2020). Characterisation of Portuguese RC Precast Industrial Building Stock. *Advances in Civil Engineering*, 1–19. <https://doi.org/10.1155/2020/7517205>
- Sagbas, G., Sheikhi Garjan, R., Sarikaya, K., & Deniz, D. (2024). Field reconnaissance on seismic performance and functionality of Turkish industrial facilities affected by the 2023 Kahramanmaraş earthquake sequence. *Bulletin of Earthquake Engineering*, 22(1), 227–254. <https://doi.org/10.1007/s10518-023-01741-8>
- Scalbi, A., Tornaghi, M. L., & Negro, P. (2018). Safecladding Project : Pseudodynamic Testing on Precast Structures With Horizontal Cladding Panels. *16th European Conference on Earthquake Engineering*, 1–12.
- Sousa, R., Batalha, N., Silva, V., & Rodrigues, H. (2020). Seismic fragility functions for Portuguese RC precast buildings. *Bulletin of Earthquake Engineering*, 1–18. <https://doi.org/10.1007/s10518-020-01007-7>
- Toniolo, G., & Lago, B. D. (2017). Conceptual design and full-scale experimentation of cladding panel connection systems of precast buildings. *Earthquake Engineering & Structural Dynamics*, 46(14), 2565–2586. <https://doi.org/10.1002/EQE.2918>
- Zoubek, B., Fischinger, M., & Isaković, T. (2016). Cyclic response of hammer-head strap cladding-to-structure connections used in RC precast building. *Engineering Structures*, 119, 135–148. <https://doi.org/10.1016/j.engstruct.2016.04.002>